Dalton Transactions

PAPER

View Article Online
View Journal | View Issue

Cite this: *Dalton Trans.*, 2017, **46**, 1996

A new adsorbent of a Ce ion-implanted metal–organic framework (MIL-96) with high-efficiency Ce utilization for removing fluoride from water†

Xuan Yang,[a,b] Shuangshuang Deng,[a] Fumin Peng*[a] and Tao Luo*[b]

Received 12th October 2016,
Accepted 10th January 2017

DOI: 10.1039/c6dt03934k

rsc.li/dalton

A novel Ce(III) ion-implanted aluminum-trimesic metal–organic framework (Ce–MIL-96) was synthesized for the first time *via* alcohol-solvent incipient wetness impregnation. Compared to previously reported Ce-contained adsorbents, the fluoride adsorption performance of the new ion-implanted metal–organic framework demonstrated much higher adsorption capacity and more efficient regeneration of Ce. In a wide pH range of 3 to 10, Ce–MIL-96 maintained constant adsorption performance for fluoride, and the residual Ce and Al in the treated solution were below the safe limits in drinking water. The maximum adsorption capacity of Ce–MIL-96 was 38.65 mg g^{-1} at 298 K. Excluding the contribution of MIL-96, the maximum adsorption capacity of Ce ions was 269.75 mg g^{-1}, which demonstrated that the service efficiency of cerium in Ce–MIL-96 is about 6 times that in Ce_2O_3, nearly 10 times that in Ce-mZrp, and double that in Mn–Ce oxides. There was no significant influence on fluoride removal by Ce–MIL-96 due to the presence of chloride, nitrate, sulfate, bicarbonate or phosphate. Moreover, the adsorption capacity of Ce–MIL-96 remained at more than 70% after nine cycles of adsorption–desorption. Due to this excellent adsorption performance and its regeneration properties, Ce–MIL-96 is a promising adsorbent for the removal of fluoride from groundwater.

1. Introduction

Fluorosis,[1] a disease caused by chronic excess intake of fluoride in drinking water, is a major challenge of human health in developing countries.[2] The permissible limit of fluoride concentration in drinking water according to WHO is 1.0 mg L^{-1}.[3] Fluoride contamination in groundwater is a worldwide problem, and many regions have reported fluoride concentrations higher than that prescribed by WHO.[3] China is also suffering from a serious fluoride epidemic caused by high concentrations of fluoride in groundwater, especially in the northern region of Anhui Province (see Fig. S1†). In view of the harmful effects of fluoride, it is essential to develop suitable methods for the removal of fluoride from water. To date, many methods have been developed to remove excess fluoride from water, including precipitation, membrane-based processes, electrocoagulation, and adsorption. Among these, adsorption of fluoride onto various materials is considered to be one of the most promising methods due to its high adsorption capacity, ease of operation and relative cost-effectiveness.[4]

Several conventional and nonconventional adsorbents, such as activated alumina,[5,6] activated carbon,[7,8] bone charcoal,[9] and natural materials,[10] have been successfully used for fluoride removal.[11,12] Among these adsorbents, activated alumina is the most common adsorbent used for defluoridation of drinking water and wastewater; however, its adsorption is often optimal at low pH values, which increases the amount of dissolved aluminium in the treated water.[13] Although bone charcoal normally has higher sorption capacity for fluoride than activated alumina, its application is limited because it is derived from animal bone, which is unacceptable for some residents of various communities on religious grounds. Recent studies have showed that rare earth materials are better able to remove some hazardous and noxious substances.[14,15] Among these, cerium can be used as a potential adsorbent material to remove fluoride from water due to its strong affinity to fluoride.[16] Therefore, many Ce-containing adsorbents have been developed, including Ce-loaded mesoporous zirconium phosphate (Ce-mZrp),[17] Mn–Ce oxides,[18] Al–Ce hybrid adsorbents,[19] and Ce-impregnated fibrous protein (Ce-FP).[20] Although these Ce -containing adsorbents show better performance for fluoride adsorption, a general weakness has emerged: these Ce-containing adsorbents demonstrate

[a]*College of Chemistry and Chemical Engineering, Anhui University, Hefei, Anhui 230039, PR China. E-mail: pengfm79@gmail.com*
[b]*Institute of Intelligent Machines, Chinese Academy of Sciences, Hefei, Anhui, 230031, P.R. China. E-mail: tluo@iim.ac.cn*

†Electronic supplementary information (ESI) available. See DOI: 10.1039/c6dt03934k

optimum adsorption of fluoride, with the highest adsorption capacities and higher adsorption rates, only at low pH value. This is especially true for Ce-FP, which reaches its maximum adsorption of fluoride at pH 3.0. In the case of regeneration, previous reports did not mention it or the results of regeneration measurements were unsatisfactory. For example, in the best result reported, Ce-mZrp adsorbent efficiently removed fluoride from water in the first four cycles; the efficiency decreased to 38% in the fifth cycle. Not only is low residual Ce a safety requirement of drinking water, but efficient use of non-renewable rare earth resources is also necessary. Therefore, the use of cerium in defluoridation with high efficiency and safety is a challenge.

Herein, we report a new adsorbent consisting of a Ce(III) ion-implanted metal–organic framework, MIL-96 (defined as Ce–MIL-96), which was designed by combining the advantage of the framework structure with the strong affinity of Ce–F for highly efficient removal of fluoride from water (Fig. 1). The Ce–MIL-96 adsorbent was synthesized for the first time *via* alcohol-solvent incipient wetness impregnation. In the Ce–MIL-96 adsorbent, the aluminium ions are fixed in the framework of MIL-96 and the cerium ions enter the internal space of MIL-96; therefore, it is difficult for Ce–MIL-96 to release aluminium and cerium ions into the treated solution. The regenerated Ce–MIL-96 adsorbent retains high adsorption capacity even for nine cycles of desorption–adsorption. Additionally, Ce(III) ions remain on the internal surface of the micropores without metal ion exchange; this is the reason that Ce(III) ions can adsorb a large amount of F^-, which shows that the service efficiency of cerium in Ce–MIL-96 is very high. Our test result was 269.75 mg g^{-1}. Meanwhile, the fluoride removal of Ce–MIL-96 remained almost constant in the pH range of 3 to 10, with much higher adsorption capacity.

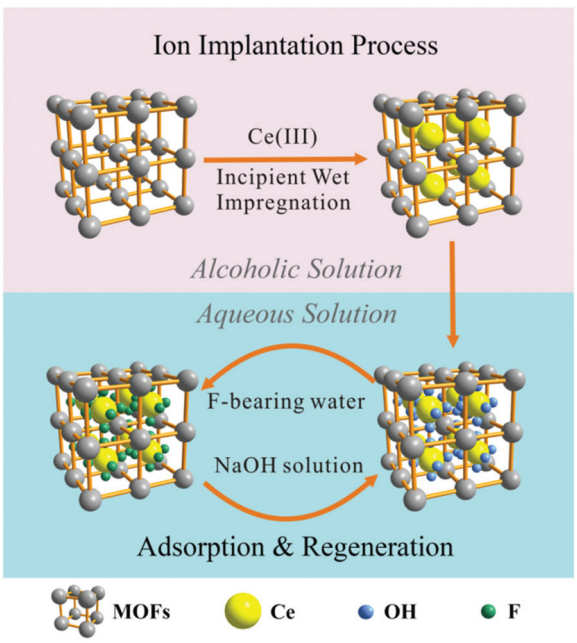

Fig. 1 Schematic of ion-implanted MOFs and their application for the removal of fluoride from water.

2. Materials and methods

2.1 Materials

1,3,5-Benzenetricarboxylic acid (H3BTC, 99%) was purchased from Aladdin Chemistry Co. Ltd. Aluminum nitrate ($Al(NO_3)_3{\cdot}9H_2O$, 98%), cerium(III) nitrate ($Ce(NO_3)_3{\cdot}6H_2O$, 98%), and other analytical reagent grade chemicals were purchased from Sinopharm Chemical Reagent Co. Ltd (Shanghai, China). All the chemicals were used in the experiments without further treatment.

The fluoride solution was prepared by dissolving NaF in deionized water.

2.2 Preparation of Ce–MIL-96

For MIL-96,[21] 20.88 g of $Al(NO_3)_3{\cdot}9H_2O$ and 4.09 g of H3BTC were dissolved in 30 mL deionized water with constant stirring for 20 min. The mixture was transferred into a 125 mL Teflon-lined stainless steel autoclave, which was then heated at 200 °C for 24 h. The white powder was washed repeatedly with deionized water and dried overnight at room temperature. Ce–MIL-96 was obtained by an alcohol-solvent incipient wet impregnation method. In a typical process, MIL-96 samples were impregnated in the same volume of $Ce(NO_3)_3$–ethanol solution for 4 hours at room temperature. After that, the product was washed with deionized water several times and dried at 60 °C overnight.

2.3 General characterization

The morphology of the sorbent was determined by scanning electron microscopy (SEM) using a QUANTA 200FG scanning electron microscope (FEI, USA). The X-ray diffraction (XRD) pattern of Ce–MIL-96 was obtained using an X'Pert X-ray diffractometer (PANalytical, Netherlands). The surface area of the samples was measured by the nitrogen adsorption–desorption method at 77 K and was evaluated by the single point BET method (Micromeritics, USA). X-ray photoelectron spectroscopy (XPS) measurements were taken using a VG ESCALAB MKII spectrometer with a Mg Ka X-ray source (1253.6 eV, 120 W) at a constant analyzer energy mode. The mass ratio of Ce(III) in Ce–MIL-96 was determined using inductively coupled plasma-atomic emission spectroscopy (Thermo Fisher Scientific icp6300, USA).

2.4 Batch adsorption experiments

In order to study the effects of different controlling parameters, such as reaction time, initial fluoride concentration, pH and competing anions, in the process of fluoride removal, the adsorption of fluoride on Ce–MIL-96 was studied by batch experiments in 250 mL plastic bottles. These bottles were shaken for a specified period of contact time in a thermostatic orbital shaker at 150 rpm at 25 ± 1 °C. The kinetic studies of the adsorption were carried out at initial fluoride concen-

trations of 6.00 and 10.00 mg L^{-1} by adding 0.050 g adsorbent to 100 mL fluoride solution, respectively. The mixtures were stirred at 150 rpm and maintained at a temperature of 25 ± 1 °C. The adsorption isotherms were acquired using 100 mL of fluoride solution with varying initial fluoride concentrations over a range of 1 to 100 mg L^{-1} in 250 mL plastic bottles, which were shaken with 0.50 g of adsorbent. After a period of 4 h, samples were withdrawn from the test bottles and filtered through a 0.2 μm syringe filter. The residual F^- concentrations of the solutions were analyzed. The adsorption capacity of the adsorbents for fluoride was determined as follows:

$$q_e = (C_o - C_e)\frac{V}{m}$$

where C_o and C_e are the initial and equilibrium fluoride concentrations of fluoride (mg L^{-1}), respectively. V is the volume of fluoride solution (mL), and m is the mass (mg) of adsorbent used in the experiments. The effect of the equilibrium pH on fluoride adsorption was investigated by adjusting the solution pH from 3 to 10 using 0.1 M HCl and 0.1 M NaOH under an initial fluoride concentration of 10 mg L^{-1}; the Ce–MIL-96 dose was 0.5 g L^{-1}. The effects of the presence of co-anions such as chloride, nitrate, sulfate, bicarbonate and phosphate on fluoride removal were investigated with a Ce–MIL-96 dosage of 0.5 g L^{-1} under a fixed fluoride concentration of 10 mg L^{-1} and initial co-anion concentrations of 10, 30, 50, and 100 mg L^{-1}, respectively.

2.5 Batch desorption experiments

Adsorbent regeneration is a very important aspect for the economy of this technology. For this purpose, 0.05 g Ce–MIL-96 was added to 100 mL fluoride solution (10.00 mg L^{-1}), and the adsorption test was conducted with shaking at 25 °C for 4 h. The fluoride-loaded adsorbent was obtained, filtered, and then shaken in 100 mL of distilled water and different concentrations of NaOH solution (0.01, 0.05, 0.10 and 0.50 M) at 25 °C for about 30 min, after which the fluoride amount desorbed into the solution was determined to calculate the removal percentage.

To test the adsorption potential of the regenerated Ce–MIL-96, nine cycles of regeneration studies were carried out under the same initial conditions.

2.6 Column experiments

To observe the practical utility of the developed method, column experiments were carried out (inner-diameter: 1.8 cm, length: 45 cm). The height of the packed Ce–MIL-96 bed was 30 cm and the volume was 76.3 mL. The groundwater used as the influent was acquired from Sanyi Town, Mengcheng County, Anhui Province, China. The characteristics of the sample are listed in Table S1.† The column was operated at an SV value of 4 h^{-1}.

2.7 Analytical methods

The solution was analyzed for residual fluoride concentration by a fluoride-selective electrode (CSF-F-1, China) connected to an ion meter (INESA PHSJ-4F, China) according to a reported method.[22] The same ion meter coupled with a pH electrode was used to measure the pH of the solution. The residual cerium and aluminum after the equilibrium were determined using inductively coupled plasma-atomic emission spectroscopy (Thermo Fisher Scientific icp6300, USA).

3. Results and discussion

Ce–MIL-96 was newly synthesized *via* an alcohol-solvent incipient wetness impregnation method. The fluoride sorption behaviors of the as-prepared Ce–MIL-96 were investigated by batch experiments, including sorption kinetics and isotherms under different initial pH values, and the presence of other ions was studied in detail. The regeneration behavior of Ce–MIL-96 was also studied. The adsorption properties of fluorine were evaluated for real F^--containing groundwater samples using column tests.

3.1 Characterization

Ce–MIL-96 and MIL-96 were synthesized for the present study to investigate the effects of Ce(III) ion implantation on the removal of fluoride. Fig. 2A shows the XRD patterns of the as-prepared MIL-96 and Ce–MIL-96, which are consistent with the simulated pattern of MIL-96.[21] Comparing the XRD patterns of MIL-96 and Ce–MIL-96, no additional peaks occur for new phases or new structures, indicating that the frame structure of MIL-96 was well retained after Ce(III) ion implantation. Fig. 2B and C show SEM images of the as-prepared MIL-96 before and after the ion implantation process; these images show that MIL-96 and Ce–MIL-96 have the same double-tined pencil morphology, indicating that the granules of MIL-96 remained intact through the ion implantation process. It can also be found that the surface of the Ce–MIL-96 particles remained smooth after the ion implantation process.

To further investigate the ion implantation process, elemental analyses of the as-obtained products were carried out. In the XPS survey spectra (shown in Fig. 3A), compared to MIL-96, there is an additional peak at 400 eV in the spectrum of Ce–MIL-96 which can be indexed to the N 1s spectrum. Fig. 3B shows the HR N 1s spectra of MIL-96 and Ce–MIL-96.

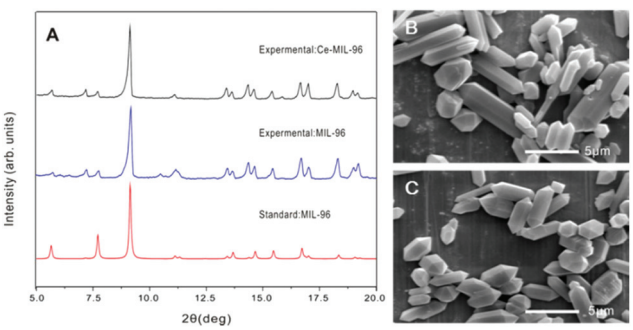

Fig. 2 (A) XRD pattern of Ce–MIL-96; (B) SEM image of MIL-96 and (C) SEM image of Ce–MIL-96.

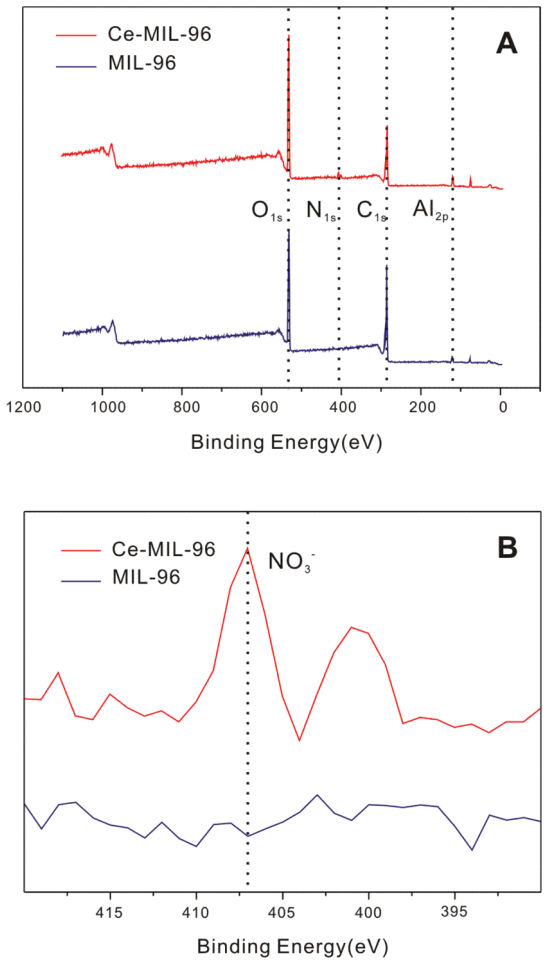

Fig. 3 XPS survey spectra (A) and high resolution N 1s spectra (B) of the as-obtained MIL-96 and Ce-MIL-96.

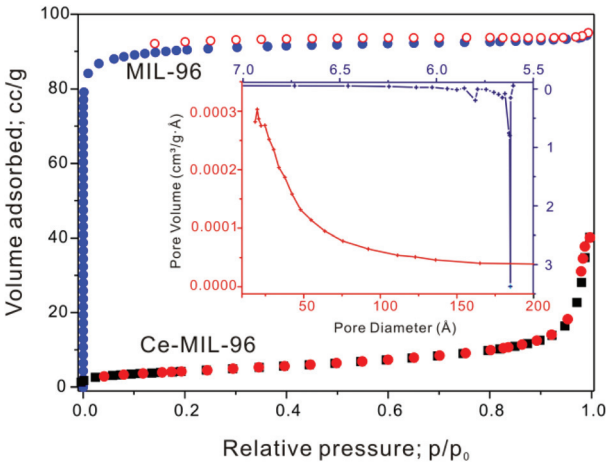

Fig. 4 Nitrogen adsorption isotherms at 77 K for MIL-96 (blue) and Ce–MIL-96 (red); the inset is the pore size distribution of MIL-96 (blue) and Ce–MIL-96 (red).

The peak centred at 407 eV indicates the presence of nitrate on the surface of Ce–MIL-96. Meanwhile, Ce element could not be found in either the XPS survey spectrum or the high resolution XPS Ce 3d spectrum (shown in Fig. S2†) of Ce–MIL-96. Interestingly, the bulk composition characterization by inductively coupled plasma-atomic emission spectroscopy (ICP-AES) revealed that the mass fraction of Ce(III) was 9.48% in the as-prepared Ce–MIL-96. Combining XPS with ICP-AES, the results indicated that the Ce(III) ions entered the internal space of MIL-96 rather than being distributed on the surface.

Fig. 4 shows the nitrogen adsorption and desorption isotherms of MIL-96 and Ce–MIL-96. According to the IUPAC classification,[23] the isotherms of MIL-96 and Ce–MIL-96 belong to type I and type II, respectively. The type I isotherm shows prominent adsorption at low relative pressure and then levels off; it is usually considered to be indicative of adsorption in micropores or monolayer adsorption due to chemisorption. In our case, nonpolar gas (nitrogen) was used for characterization. Hence, chemisorption was unlikely, and a reasonable interpretation would associate the type I isotherm with microporosity. Due to the type I isotherm, the Horvath–Kawazoe method was employed to calculate the pore size distribution (PSD). The PSD result of MIL-96 (shown in the inset of Fig. 4) indicated that the median pore size was about 5.6 Å, which is consistent with the above analysis. The type II isotherm is the characteristic form of an isotherm obtained for a non-porous or macroporous adsorbent. The type II isotherm represents unrestricted monolayer–multilayer adsorption. In this type of isotherm, the beginning point of the almost linear middle section of the isotherm is often taken to indicate the stage at which monolayer coverage is complete and multilayer adsorption is about to begin. In the case of the Ce–MIL-96 adsorption isotherm, the beginning point was at very low relative pressure, which indicated that Ce–MIL-96 exhibited the adsorption properties of a non-porous solid with a small BET surface area. The PSD of Ce–MIL-96 calculated by the BJH method indicated that the micropores of MIL-96 did not exist in Ce–MIL-96. The calculated BET surface area of Ce–MIL-96 was 18.28 $m^2 g^{-1}$, far less than the value of MIL-96 (272.02 $m^2 g^{-1}$). The most reasonable explanation is that implanted Ce(III) ions occupied the micropores of MIL-96 and prevented nitrogen from entering the internal space of the framework, resulting in adsorption of nitrogen onto the external surface of Ce–MIL-96 rather than the internal surface.

To determine the status of the Ce(III) ions in the Ce–MIL-96 framework, a reverse ion implantation experiment was carried out. As-prepared MIL-96 and Ce–MIL-96 were immersed in pure alcohol for 4 hours at room temperature. After separation, the alcohol solutions were characterized by ICP-AES. The results (listed in Table S2†) demonstrated that there was no Al element in the solutions treated with MIL-96 and Ce–MIL-96. Ce was found in the solution treated with Ce–MIL-96. These results indicated two facts: Al was stable in the MOF, and Ce did not exchange with Al in the framework of MIL-96 during the ion implantation process. Therefore, the Ce(III) ions should be found on the internal surface of the micropores without metal ion exchange. The original MIL-96 and Ce–MIL-96

samples were also characterized by FT-IR spectroscopy. The result (shown in Fig. S3†) demonstrated that there were no additional peaks or band shifts in the FTIR spectrum of Ce–MIL-96 compared to the spectrum of MIL-96, which confirmed the conclusion of the reverse ion implantation experiment mentioned above.

3.2 Effect of the amount of implanted ions

The effect of the amount of implanted Ce(III) on the removal of fluoride is shown in Table S3.† The initial concentrations of Ce(III) were varied from 0.001 to 0.5 mol L^{-1}. It can be found from the table that the fluoride adsorption capacity of Ce–MIL-96 increased with increasing amount of the implanted Ce(III), reaching the maximum at the initial Ce(III) concentration of 0.2 mol L^{-1}, and then decreased as the amount of implanted Ce(III) increased further. Hence, the sample with the implantation process at the initial Ce(III) concentration of 0.2 mol L^{-1} was chosen to investigate the adsorption properties of Ce–MIL-96.

3.3 Adsorption kinetics

In order to determine the equilibration time for the maximum adsorption of fluoride and to determine the kinetics of the adsorption process, kinetics studies of the adsorption of fluoride from synthetic solutions were carried out; the results are shown in Fig. 5. It can be seen from the figure that the removal of fluoride increased with contact time. Within the first 10 and 40 min of the contact time, nearly 90% removal of fluoride was achieved with initial fluoride concentrations of 6 and 10 mg L^{-1}, respectively. Only the remaining 10% removal occurred in the following 4 h. It is clear that the time to achieve equilibrium adsorption is related to the initial fluoride concentration.

To identify the rate and kinetics of the adsorption of fluoride on Ce–MIL-96, the kinetics data were analyzed using the following four simplified kinetic models: pseudo-first-order, pseudo-second-order, Weber and Morris intraparticle diffusion model and Bangham's pore diffusion model.

The Lagergren's rate equation is one of the most widely used rate equations to describe the adsorption of an adsorbate from the liquid phase.[24] The linear form of the pseudo-first-order rate expression of Lagergren is given as:

$$\log(q_e - q_t) = \log q_e - \frac{k_f}{2.303}t$$

where q_e and q_t are the amounts of fluoride adsorbed per unit mass of adsorbent at equilibrium and time t, respectively, and k_f is the rate constant (min^{-1}). Fig. 6A shows a plot of the linearized form of the pseudo-first-order model at the two initial concentrations studied. Kinetic parameters, along with correlation coefficients of the kinetic models, are listed in Table 1. Although the plots were found to be linear, with good correlation coefficients (>0.90), the calculated q_e values do not give reasonable values; therefore, the adsorption of fluoride on Ce–MIL-96 does not fit the pseudo-first-order model.

The adsorption kinetics was described as a pseudo-second-order process:[25]

$$\frac{t}{q_t} = \frac{1}{k_s q_e^2} + \frac{1}{q_e}t$$

where q_e and q_t have the same meaning as in the Lagergren first order rate expression, and k_s is the rate constant for the pseudo-second-order kinetics. The plots of t/q_t *versus* t are shown in Fig. 6B. The calculated q_e values are closer to the experimental data than the calculated values of the pseudo-first-order model. Meanwhile, the values of the correlation coefficient (R^2) for the pseudo-second-order model are relatively higher than the values for the pseudo-first-order model. Therefore, the adsorption of fluoride can be approximated more favorably by the pseudo-second-order model.

The mechanism of adsorption on porous material is generally considered to involve a sequential progression through

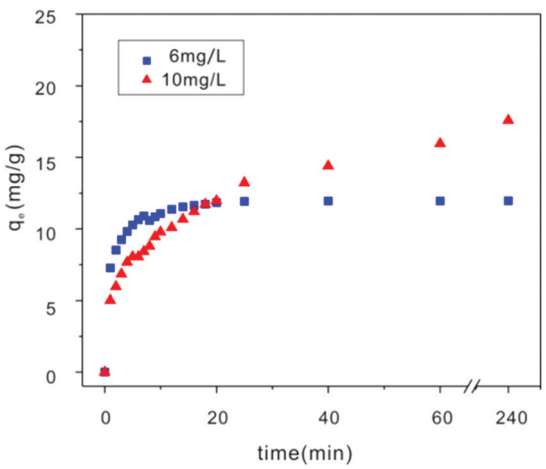

Fig. 5 Effects of contact time and initial fluoride concentration on fluoride adsorption (temperature = 298 K; Ce–MIL-96 dose = 0.5 g L^{-1}; pH = 7.0).

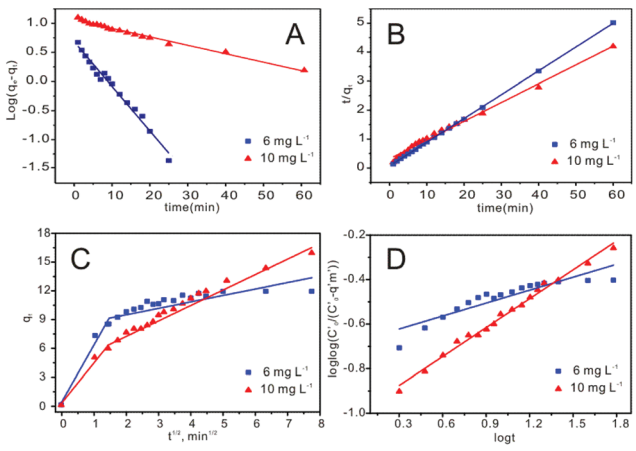

Fig. 6 Kinetic modeling of the adsorption of fluoride on Ce–MIL-96: (A) pseudo-first-order kinetic plots; (B) pseudo-second-order kinetic plots; (C) Weber and Morris intraparticle diffusion plots; and (D) Bangham pore diffusion plots.

Table 1 Comparison of pseudo-first-order, pseudo-second-order, Weber and Morris, and Bangham's model parameters and calculated $q_{e(cal)}$ and experimental $q_{e(exp)}$ values for different initial fluoride concentrations

Pseudo-first-order model				
C_o (mg L^{-1})	$q_{e(exp)}$ (mg L^{-1})	k_f (min^{-1})	$q_{e(cal)}$ (mg L^{-1})	R^2
6	11.95	0.19	5.59	0.961
10	15.96	0.04	11.92	0.952
Pseudo-second-order model				
C_o (mg L^{-1})	$q_{e(exp)}$ (mg L^{-1})	k_s (min^{-1})	$q_{e(cal)}$ (mg L^{-1})	R^2
6	11.95	0.10	12.18	0.999
10	15.96	0.01	15.43	0.992
Weber and Morris model				
C_o (mg L^{-1})	K_{ip1} (mg g^{-1} $min^{-0.5}$)	R^2	K_{ip2} (mg g^{-1} $min^{-0.5}$)	R^2
6	6.26	0.954	7.83	0.886
10	4.36	0.961	3.52	0.990
Bangham's model				
C_o (mg L^{-1})	K_0 (mL (g L^{-1})$^{-1}$)		α	R^2
6	48.35		0.22	0.999
10	27.38		0.39	0.992

three steps: (i) mass diffusion through the external boundary layer film of liquid surrounding the outside of the solid; (ii) adsorption on the solid surface (internal or external); (iii) intraparticle diffusion either by a pore diffusion process through the liquid filled pores or by a solid surface diffusion mechanism.[26] The following models were discussed to address the diffusion mechanisms of adsorption on Ce–MIL-96.

The concentration dependence of the rate of sorption is often used to analyze the nature of the rate-determining step, and the use of the intraparticle diffusion model has been greatly explored in this regard. This is represented by the following equation of the Weber and Morris model:[27]

$$q_t = k_{ip} t^{1/2} + C$$

where C is related to the thickness of the boundary layer and k_{ip} is the intraparticle diffusion rate constant. The Weber and Morris plots of fluoride adsorption on Ce–MIL-96 are shown in Fig. 6C. If the adsorption is controlled by the intraparticle diffusion process, a plot of q_t *versus* $t^{1/2}$ gives a straight line. From the plots in Fig. 6C, it can be clearly seen that there are two separate zones: the first linear portion (phase I) and the second linear portion (phase II). The slope of the linear portion indicated the rate of the adsorption. In phase I, the sharp portion was attributed to the immediate utilization of the most readily available adsorbing sites on the external surface of Ce–MIL-96. Phase II was attributed to very slow diffusion of fluoride from the surface site into the inner pores. The values of k_{ip1} and k_{ip2} (intraparticle diffusion rate constants for phase I and phase II) were obtained from the slopes of the linear plots and are listed in Table 1. It is clear from the k_{ip} values that k_{ip1} (7.83 at 6 mg L^{-1} and 4.36 at 10 mg L^{-1}) is higher than k_{ip2} (6.26 at 6 mg L^{-1} and 3.52 at 10 mg L^{-1}); this indicates that the initial step is rapid, followed by a slow step.

Bangham's equation has been used to describe pore diffusion during adsorption processes:[28]

$$\log\left(\frac{C_i}{C_i - q_t m}\right) = \log\left(\frac{k_0}{2.303V}\right) + \alpha \log t$$

where C_i is the initial concentration of the adsorbate (mmol L^{-1}), V is the volume of the solution (mL), m is the weight of the adsorbent (g L^{-1}), q_t (mmol g^{-1}) is the amount of adsorbate retained at time t, and α (less than 1) and k_0 are constants. The plots were found to be linear, with good correlation coefficients (>0.99) (see Fig. 6D); this indicates the applicability of Bangham's model and therefore indicates that the adsorption of fluoride onto Ce–MIL-96 was controlled by pore diffusion.

3.4 Adsorption isotherm

The effect of the initial concentration on the adsorption capacity of the adsorbents for fluoride was studied at different initial fluoride concentrations (C_0 = 1–100 mg L^{-1}), and the results are shown in Fig. 7A. The Langmuir and Freundlich models are the most commonly used isotherms to represent the adsorption of a component from the liquid phase onto a solid phase. The Langmuir equation may be expressed as:

$$\frac{C_e}{q_e} = \frac{1}{q_m K_L} + \frac{C_e}{q_m}$$

where q_m is the maximum amount of fluoride per unit weight of adsorbent to form a complete monolayer on the surface

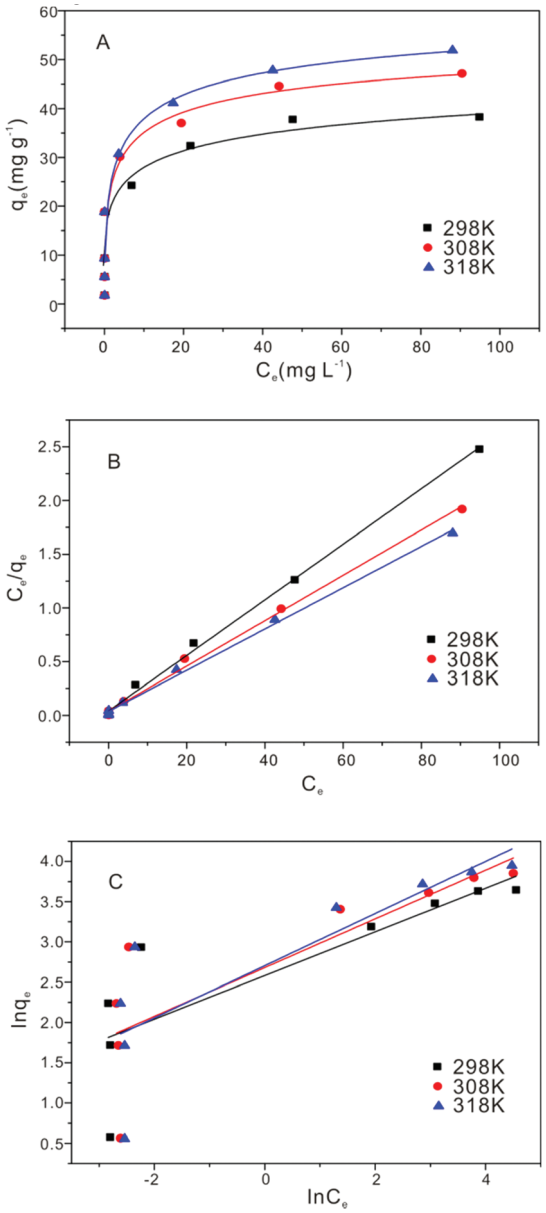

Fig. 7 Isotherm of fluoride adsorption on Ce–MIL-96 (A), Langmuir (B), Freundlich (C) (contact time = 4 h; MIL-96 dose = 0.5 g L^{-1}; pH = 7).

bound at high C_e, while K_L is a constant related to the affinity of the binding sites. q_e represents the particle limiting adsorption capacity when the surface is fully covered with solution. The plots of C_e/q_e as a function of q_e for the adsorption of fluoride are shown in Fig. 7B. The Freundlich equation may be expressed as:

$$\ln q_e = \frac{1}{n}\ln C_e + \ln K_F$$

where K_F and $1/n$ are the Freundlich constants; they are considered to be relative indicators of adsorption capacity and adsorption intensity, respectively. The Freundlich plots between $\ln q_e$ and $\ln C_e$ for the adsorption of fluoride are shown in Fig. 7C.

The derived parameters from the least square fittings of the Langmuir and Freundlich equations are given in Table 2. It is evident that the Langmuir model is slightly better fitted to the experimental data (correlation coefficient = 0.99). The values of q_m calculated by the Langmuir isotherm were all close to experimental values at given temperatures.

It is worthwhile to compare the fluoride adsorption of Ce–MIL-96 with that of pure MIL-96. From this study, it is clear that the q_{max} value for Ce–MIL-96 is around 1.22 times higher than that of MIL-96, which indicates a more favorable adsorption. The implanted Ce(III) ions play important roles in the better fluoride adsorption characteristics of Ce–MIL-96.

3.5 Effect of pH on adsorption

The pH of the solution is an important parameter which significantly affects the extent of fluoride adsorption. The effects of pH on fluoride removal by Ce–MIL-96 was investigated in the pH range of 3 to 10 with an initial concentration of 10 mg L^{-1}. The results of the effect of pH on fluoride adsorption onto Ce–MIL-96, NA and AA are shown in Fig. 8. It is clear that the fluoride removal of Ce–MIL-96 remained almost constant in the pH range of 3 to 10, with much higher adsorption capacity than AA and NA. In contrast, the maximum fluoride adsorption capacities of AA and NA were reached at pH 3.0. In the wide pH range of 4 to 10, the fluoride

Table 2 Langmuir and Freundlich isotherm parameters for fluoride adsorption on Ce–MIL-96

	Langmuir model			Freundlich model		
	q_m (mg g^{-1})	k_L (L mg^{-1})	R^2	k_F (g mg^{-1})	$1/n$	R^2
298 K	38.65	0.65	0.997	13.24	0.27	0.621
308 K	45.05	0.60	0.996	14.60	0.30	0.629
318 K	52.08	0.54	0.997	14.95	0.32	0.652

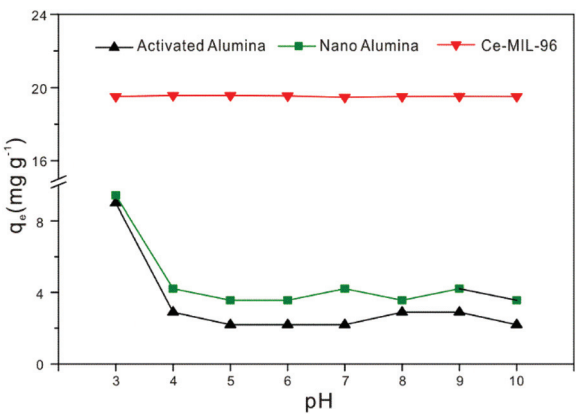

Fig. 8 Effects of pH on the fluoride adsorption capacity of Ce–MIL-96, NA and AA.

adsorption capacities of AA and NA remained at lower levels, less than the half of the maximum capacity.

The residual aluminum and cerium concentrations of the solutions treated with Ce–MIL-96 were measured to be 0.142 and 0.218 mg L^{-1}, respectively. It can be seen that the Ce–MIL-96 treated solution has very low concentrations of residual aluminum and cerium ions; this is because the aluminum ions are fixed in the framework of MIL-96 and the cerium ions entered the internal space of MIL-96. It is difficult for Ce–MIL-96 to release aluminum and cerium ions into the treated solution. The results of a comparative stability experiment (listed in Table S4†) show that Ce–MIL-96 has the same high stability as MIL-96. The results indicate that Ce–MIL-96 is a promising candidate for the removal of fluoride from drinking water due to its high stability in the course of its use.

3.6 Competitive adsorption

In this study, the individual effects of co-existing ions, including chloride (Cl^-), nitrate (NO_3^-), sulfate (SO_4^{2-}), bicarbonate (HCO_3^-) and phosphate (PO_4^{3-}), were investigated with concentrations of the anions ranging from 10 to 100 mg L^{-1}; the initial concentration of the fluoride was maintained at 10 mg L^{-1} at a temperature of 25 °C. The pH was not controlled when adding different competing anions to the fluoride solution. The effects of the anions on the removal of fluoride are shown in Fig. 9. From the adsorption experiment results, it can be observed that these competing anions show no significant effects on fluoride removal. Although the concentration of the competing PO_4^{3-} anion was as high as 100 mg L^{-1}, the fluoride removal efficiency only decreased from 92% to 80%. This indicates that Ce–MIL-96 possesses excellent anti-interference abilities against competing anions, resulting from the unique size-selective ability of the micropores in the MIL-96 structure. The results of a DFT simulation (Fig. S4†) performed with the Gaussian 03 package show that the sizes of the clusters $NO_3^-(H_2O)$, $SO_4^{2-}(H_2O)_2$, $HCO_3^-(H_2O)$ and $PO_4^{3-}(H_2O)_2$ are 6.06, 8.17, 6.02, and 7.95 Å, respectively; these are larger than the median pore width of MIL-96. The median pore width of MIL-96 is 5.62 Å. Therefore, these anions cannot enter the internal pores of MIL-96, ensuring its high selectivity for fluoride.

To investigate the feasibility of Ce–MIL-96 for the removal of fluoride from groundwater, high fluoride-bearing groundwater sampled from Sanyi Town, Mengcheng County, Anhui Province, China was treated with Ce–MIL-96 (Ce–MIL-96 dose 0.5 g L^{-1}, temperature 298 K). Through adsorption by Ce–MIL-96, nearly all the fluoride in the groundwater was removed. The fluoride concentration decreased from 3.16 mg L^{-1} (before treatment) to 0.09 mg L^{-1} (after treatment), thereby meeting the water quality standard for fluoride concentration. Detailed characteristics of the groundwater samples before and after treatment with Ce–MIL-96 are given in Table S1.† This strongly suggests that this adsorbent is suitable for drinking water treatment.

3.7 Thermodynamic parameters

The thermodynamic parameters of adsorption standard free energy change ($\Delta G°$), standard enthalpy change ($\Delta H°$), and standard entropy change ($\Delta S°$) for the adsorption process were calculated using the following equations. The standard free energy change ($\Delta G°$) is given by the equation:[29]

$$\Delta G° = -RT \ln k_0$$

where $\Delta G°$ is the standard free energy change of adsorption (kJ mol^{-1}), T is the temperature in Kelvin, R is the universal gas constant (8.314 J mol^{-1} K^{-1}) and k_0 is the thermodynamic equilibrium constant, which is equal to $q_m \times K_T$ of the Langmuir isotherm.

The standard enthalpy change ($\Delta H°$) and standard entropy change ($\Delta S°$) were calculated using the equation:[29]

$$\ln k_0 = \frac{\Delta S°}{R} - \frac{\Delta H°}{RT}$$

where ($\Delta H°$) is the standard enthalpy change (kJ mol^{-1}) and ($\Delta S°$) is the standard entropy change (kJ mol^{-1} K^{-1}). The values of $\Delta H°$ and $\Delta S°$ were obtained from the slopes and intercepts of $\ln k_0$ against $1/T$ (Fig. 10). These values were observed to be 4526 J mol^{-1} and 42 J mol^{-1} K^{-1}, respectively.

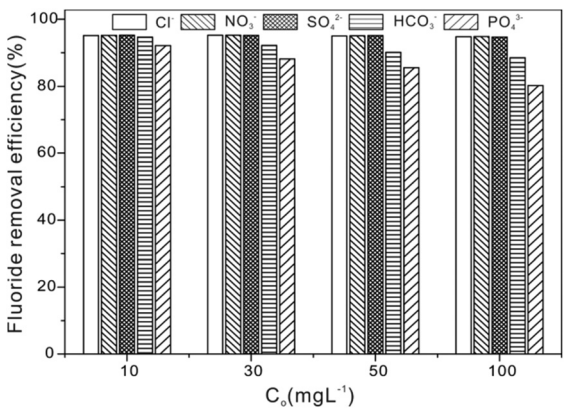

Fig. 9 Effects of competing anions on the fluoride removal efficiency of Ce–MIL-96 (temperature = 298 K; contact time = 4 h; adsorbent dose = 1 g L^{-1}; initial fluoride concentration = 10 mg L^{-1}).

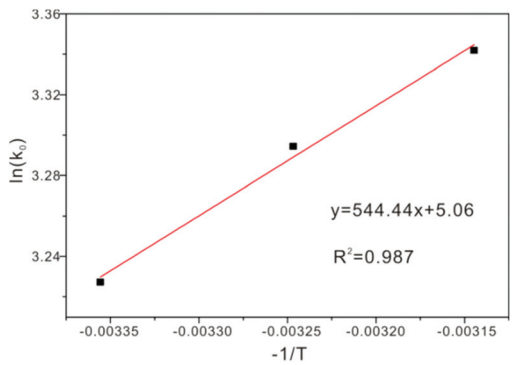

Fig. 10 Van't Hoff plot for the removal of fluoride by Ce–MIL-96.

The negative values of ΔG°, −8.00, −8.44, and −8.84 kJ mol^{-1}, at the three temperatures studied indicated the feasibility and spontaneity of the sorption reaction. The positive value of ΔH° for fluoride adsorption on Ce–MIL-96 indicates that the reaction is exothermic, and the increase in temperature favors adsorption.

3.8 Batch desorption experiments

After adsorption, the Ce–MIL-96 bearing fluoride should be either safe for disposal or suitably treated for regeneration. The desorption studies are shown in Fig. 11. It is evident that there is practically no release of fluoride in deionized water medium. However, using 0.01, 0.05, 0.10 and 0.50 M NaOH, respective desorption ratios of 83.42%, 82.12%, 43.26% and 31.12% were obtained. It was found that similarly high efficiencies were obtained using 0.01 and 0.05 M NaOH. Considering the negative effects of alkaline residues on the structure of Ce–MIL-96, 0.01 M NaOH was considered to be optimal for the regeneration process.

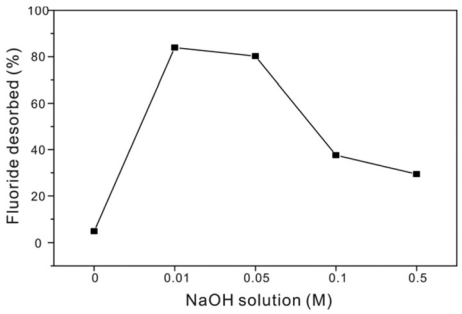

Fig. 11 % fluoride desorbed at various concentrations of NaOH (temperature = 25 °C; adsorbent dose = 0.5 g L^{-1}; initial fluoride concentration = 10 mg L^{-1}).

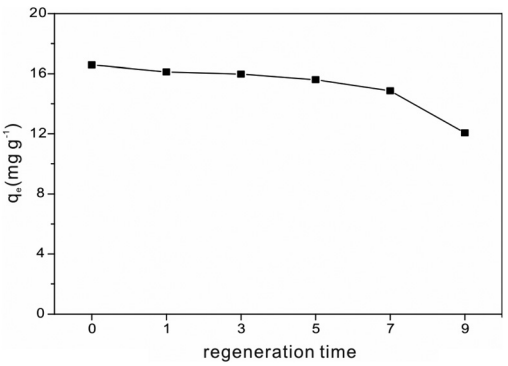

Fig. 12 Regeneration test of Ce–MIL-96 (temperature = 298 K; contact time = 4 h; adsorbent dose = 0.5 g L^{-1}; initial fluoride concentration = 10 mg L^{-1}).

To verify the regeneration performance of Ce–MIL-96, more cycles of adsorption–desorption studies were carried out while maintaining the same initial conditions. The results are shown in Fig. 12. The regenerated Ce–MIL-96 adsorbent retains high adsorption capacity, even for nine cycles of desorption–adsorption.

3.9 Mechanism of removing fluoride

To understand the function of the implanted Ce(III) ions on the removal of fluoride, the fluoride adsorption capacity of Ce–MIL-96 (with 4 wt% Ce) was compared with some efficient Ce-contained adsorbents reported previously, including Ce_2O_3, Ce-mesoporous ZrP (Ce-mZrp), and Mn–Ce oxide. The three typical Ce-contained adsorbents represent the three typical modes of cerium use: exclusive use, loading on porous materials, and dopant.

For comparison, the maximum adsorption capacities of the Ce-contained adsorbents should be converted into the same standard values to cerium *via* the equation:

$$q_{m(Ce)} = \frac{q_{m(total)} - q_{m(non\text{-}Ce)}}{W_{Ce}}$$

where $q_{m(total)}$, $q_{m(non\text{-}Ce)}$ and $q_{m(Ce)}$ represent the maximum adsorption capacity related to the mass of adsorbent, the mass of the part of the adsorbent without cerium, and the mass of cerium contained in the adsorbent, respectively. W_{Ce} is the weight content of cerium in the adsorbent. By this conversion, the $q_{m(Ce)}$ values (listed in Table 3) of Ce–MIL-96, Ce_2O_3, Ce-mZrp, and Mn–Ce oxide are 269.75, 43.22, 27.95, and 128.76 mg g^{-1}, respectively, which indicates that the service efficiency of cerium in Ce–MIL-96 is about 6 times that in Ce_2O_3, nearly 10 times that in Ce-mZrp, and double that in Mn–Ce oxides. It is obvious that the ion-implanted Ce in the framework of MIL-96 showed higher efficiency for the removal of fluoride compared to the other three modes of Ce use. According to the literature,[30] the higher efficiency can be attributed to the synergistic effects between Ce(III) and MIL-96. The Ce(III) ions dispersed in the micropores of MIL-96, which resulted in higher fluoride adsorbing activity and more adsorption sites. Meanwhile, the synergistic effect enhanced the Ce–MIL-96 stability and extended the pH range for the removal of fluoride. To further investigate the removal mechanism, FT-IR spectroscopy was used to characterize the Ce–MIL-96

Table 3 Comparison of the adsorption capacities of fluoride on some efficient Ce-containing adsorbents

Adsorbent	Solution pH	$q_{m(total)}$ (mg g^{-1})	$q_{m(non\text{-}Ce)}$ (mg g^{-1})	W_{Ce} (wt%)	$q_{m(Ce)}$ (mg g^{-1})	Ref.
Ce–MIL-96	3—10	39.97	29.18	4.00	269.75	This study
Ce_2O_3	6	36.9	—	85.37	43.22	18
Ce-mZrp	6	20.5	13.7	24.33	27.95	17
Ce–Mn oxide	6	79.5	2.8	59.57	128.76	18

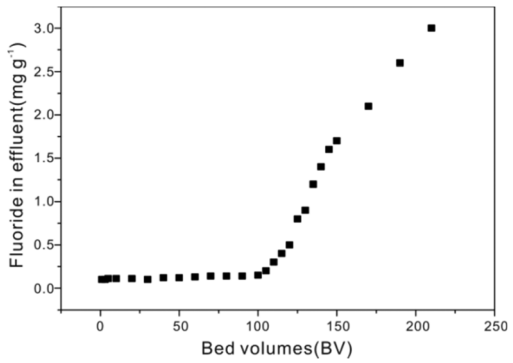

Fig. 13 Column tests of Ce–MIL-96 adsorbent particles in the treatment of real F^--containing groundwater (sampled from Sanyi Town, Mengcheng County, Anhui Province, China).

powder at three different stages: before adsorption of fluoride, after adsorption of fluoride and after regeneration (shown in Fig. S5†). In the wavenumber range from 1050 to 1090 cm^{-1}, Ce–MIL-96 showed a peak at 1067 cm^{-1}, corresponding to the bending vibration of Ce–OH. This peak disappeared after adsorption of fluoride and returned after regeneration treatment with NaOH solution; this indicated that the adsorption of fluoride on Ce–MIL-96 depended on ion exchange with –OH bound to Ce in the pores of the MOF.

3.10 Column experiments

The column test results are shown in Fig. 13. With an influent fluoride concentration of 3.16 mg L^{-1} and a pH of 7.9, about 140 BVs of groundwater, corresponding to a SVs of 4 h^{-1}, was treated before the F- in the effluent reached 1.5 mg L^{-1} (WHO standard).

4. Conclusions

A novel Ce–MIL-96 adsorbent with high sorption capacity for fluoride was successfully prepared *via* incipient wetness impregnation. Adsorption isotherms showed that the maximum adsorption capacity of Ce–MIL-96 for fluoride was 38.65 mg g^{-1} at 298 K, according to the Langmuir fitting. The adsorption isotherm fitted well with the Langmuir model. The adsorption of fluoride on Ce–MIL-96 was very fast within the first 20 min; adsorption equilibrium was achieved after 4 h, and the adsorption process followed pseudo-second-order kinetics with controlled pore diffusion. The pH conditions of the initial solution influenced the fluoride removal by Ce–MIL-96 only slightly in a wide pH range of 3 to 10, while the concentrations of residual aluminum and cerium in the treated solution were below the safe limits in drinking water. There were no significant influences on fluoride removal by Ce–MIL-96 due to the presence of chloride, nitrate, sulfate, bicarbonate and phosphate. The results of regeneration tests demonstrated that 0.01 M NaOH was optimal for desorbing the F^--loaded Ce–MIL-96. Column studies showed that Ce–MIL-96 was efficient in the treatment of real F^--containing groundwater from Mengcheng County, China. The results of the present study indicate that Ce–MIL-96 has good potential to be used as an effective adsorbent in water treatment for defluoridation.

Acknowledgements

We thank the National Natural Science Foundation of China (Grant No. 21407001 and U1432140).

Notes and references

1 J. J. Murray, *Br. Dent. J.*, 1973, **134**, 347–350.
2 M. Amini, K. Mueller, K. C. Abbaspour, T. Rosenberg, M. Afyuni, K. N. Moller, M. Sarr and C. A. Johnson, *Environ. Sci. Technol.*, 2008, **42**, 3662–3668.
3 WHO, London, UK, 2006.
4 M. Mohapatra, S. Anand, B. K. Mishra, D. E. Giles and P. Singh, *J. Environ. Manage.*, 2009, **91**, 67–77.
5 S. Ghorai and K. K. Pant, *Chem. Eng. J.*, 2004, **98**, 165–173.
6 W. X. Gong, J. H. Qu, R. P. Liu and H. C. Lan, *Chem. Eng. J.*, 2012, **189**, 126–133.
7 M. Srimurali, A. Pragathi and J. Karthikeyan, *Environ. Pollut.*, 1998, **99**, 285–289.
8 Meenakshi and R. C. Maheshwari, *J. Hazard. Mater.*, 2006, **137**, 456–463.
9 P. D. Nemade, A. V. Rao and B. J. Alappat, *Water Sci. Technol.*, 2002, **2**, 311–317.
10 Y. Shan and H. M. Guo, *Chem. Eng. J.*, 2013, **223**, 183–191.
11 X. Fan, D. J. Parker and M. D. Smith, *Water Res.*, 2003, **37**, 4929–4937.
12 A. K. Yadav, C. P. Kaushik, A. K. Haritash, A. Kansal and N. Rani, *J. Hazard. Mater.*, 2006, **128**, 289–293.
13 A. Lopez Valdivieso, J. L. Reyes Bahena, S. Song and R. Herrera Urbina, *J. Colloid Interface Sci.*, 2006, **298**, 1–5.
14 Z. He, S. Tian and P. Ning, *J. Rare Earths*, 2012, **30**, 563–572.
15 C.-M. Hung, J.-C. Lou and C.-H. Lin, *Chemosphere*, 2003, **52**, 989–995.
16 F. Luo and K. Inoue, *Solvent Extr. Ion Exch.*, 2004, **22**, 305–322.
17 S. S. Dash, M. K. Sahu, E. Sahu and R. K. Patel, *New J. Chem.*, 2015, **39**, 7300–7308.
18 S. B. Deng, H. Liu, W. Zhou, J. Huang and G. Yu, *J. Hazard. Mater.*, 2011, **186**, 1360–1366.
19 H. Liu, S. Deng, Z. Li, G. Yu and J. Huang, *J. Hazard. Mater.*, 2010, **179**, 424–430.
20 H. Deng and X. Yu, *Chem. Eng. J.*, 2012, **184**, 205–212.
21 T. Loiseau, L. Lecroq, C. Volkringer, J. Marrot, G. Ferey, M. Haouas, F. Taulelle, S. Bourrelly, P. L. Llewellyn and M. Latroche, *J. Am. Chem. Soc.*, 2006, **128**, 10223–10230.
22 Q. Liu, H. M. Guo and Y. Shan, *J. Fluorine Chem.*, 2010, **131**, 635–641.

23 K. S. W. Sing, D. H. Everett, R. A. W. Haul, L. Moscou, R. A. Pierotti, J. Rouquerol and T. Siemieniewska, *Pure Appl. Chem.*, 1985, **57**, 603–619.
24 S. Ghorai and K. K. Pant, *Sep. Purif. Technol.*, 2005, **42**, 265–271.
25 Y. S. Ho and G. McKay, *Process Biochem.*, 1999, **34**, 451–465.
26 W. H. Cheung, Y. S. Szeto and G. McKay, *Bioresour. Technol.*, 2007, **98**, 2897–2904.
27 J. C. M. W. J. Weber Jr., *J. Sanit. Eng. Div.*, 1963, **89**, 31–59.
28 C. Aharoni and M. Ungarish, *J. Chem. Soc., Faraday Trans.*, 1977, **73**, 456–464.
29 M. Yang, T. Hashimoto, N. Hoshi and H. Myoga, *Water Res.*, 1999, **33**, 3395–3402.
30 J. Song, Z. Luo, D. K. Britt, H. Furukawa, O. M. Yaghi, K. I. Hardcastle and C. L. Hill, *J. Am. Chem. Soc.*, 2011, **133**, 16839–16846.